A Hierarchical Strategy for Reconstruction of 3D Acetabular Surface Models from 2D Calibrated X-Ray Images

Steffen Schumann[1], Moritz Tannast[2], Mathias Bergmann[3], Michael Thali[4], Lutz-P. Nolte[1], and Guoyan Zheng[1]

[1] Institute for Surgical Technology and Biomechanics, University of Bern, Switzerland
[2] Inselspital, Orthopaedic Department, University of Bern, Switzerland
[3] Institute of Anatomy, University of Bern, Switzerland
[4] Institute of Forensic Medicine, University of Bern, Switzerland

Abstract. Recent studies have shown the advantage of performing range of motion experiments based on three-dimensional (3D) bone models to diagnose femoro-acetabular impingement (FAI). The relative motion of pelvic and femoral surface models is assessed dynamically in order to analyze potential bony conflicts. 3D surface models are normally retrieved by 3D imaging modalities like computed tomography (CT) or magnetic resonance imaging (MRI). Despite the obvious advantage of using these modalities, surgeons still rely on the acquisition of planar X-ray radiographs to diagnose orthopedic impairments like FAI. Although X-ray imaging has advantages such as accessibility, inexpensiveness and low radiation exposure, it only provides two-dimensional information. Therefore, a 3D reconstruction of the hip joint based on planar X-ray radiographs would bring an enormous benefit for diagnosis and planning of FAI-related problems. In this paper we present a new approach to calibrate conventional X-ray images and to reconstruct a 3D surface model of the acetabulum. Starting from the registration of a statistical shape model (SSM) of the hemi-pelvis, a localized patch-SSM is matched to the calibrated X-ray scene in order to recover the acetabular shape. We validated the proposed approach with X-ray radiographs acquired from 6 different cadaveric hips.

1 Introduction

Three-dimensionally (3D) reconstructed bone shapes are an important means for clinical diagnosis of orthopedic impairments [1][2]. 3D bone shapes are normally retrieved from computed-tomography (CT) datasets by performing semi-automatic segmentation. However, in order to reduce costs and to keep the radiation exposure to the patient low, the acquisition of planar X-ray radiographs is in general preferred to CT-scans. Based on the 2D X-ray projections of the anatomy, important clinical parameters are estimated to make a diagnosis or to plan a surgical treatment.

P. Abolmaesumi et al. (Eds.): IPCAI 2012, LNAI 7330, pp. 74–83, 2012.

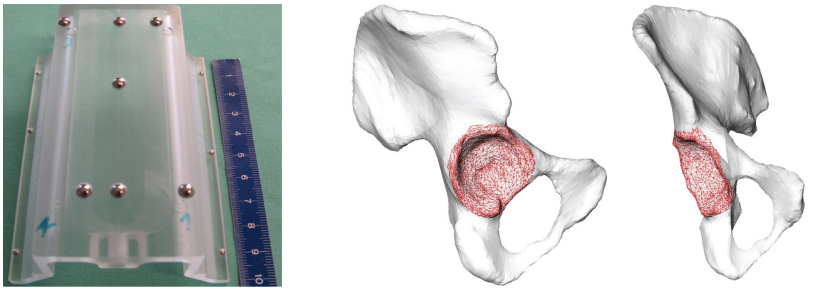

Fig. 1. Left: Topview of calibration phantom showing top layer with seven fiducials. Right: Definition of acetabulum patch based on mean hemi-pelvis model.

X-ray images also play a major role in the diagnosis of femoro-acetabular impingement (FAI). In order to identify possible bony conflicts between acetabular structures of the pelvis and the proximal femur, an anterior-posterior (AP) and a cross-table axial X-ray radiograph are normally acquired [3]. Special attention has to be paid to the correct alignment of the patient's hip joint with respect to the image plane. Otherwise, wrong interpretations or miscalculations could occur [4]. Moreover, X-ray projections only provide two-dimensional (2D) information. Recent trials have shown an improvement in FAI diagnosis and planning by performing range of motion studies using 3D surface models of the pelvis and the proximal femur, which are normally derived from 3D imaging modalities such as CT or MRI [4,5]. However, in clinical routine, CT-scans are only acquired in rare cases of severe pelvic deformations [6] and magnetic-resonance imaging (MRI) poses a challenge for 3D bone segmentation. In this paper, we propose to derive 3D information from two X-ray images.

In previous work we have already successfully shown that it is possible to reconstruct the 3D surface of the proximal femur from calibrated X-ray images with a sufficient accuracy [7]. In the following, we are going to describe a method to reconstruct the 3D shape of the acetabulum from biplanar radiographs. The major challenge is thereby to recover the correct fossa depth and the rim curvatures. Besides the development of a small-sized mobile X-ray calibration phantom, a hierarchical strategy was developed to precisely reconstruct the shape of the acetabulum. Our approach was validated based on six pairs of X-ray radiographs, acquired from six dry cadaveric bones.

2 Materials and Methods

2.1 Calibration

A calibration step is required in order to extract quantitative information from 2D X-ray projections. This step is accomplished by integrating a mobile phantom (Fig. 1) into the X-ray imaging process. The phantom is designed to have 16 fiducials of two different dimensions embedded, arranged in three different planes.

The 3D locations of these fiducials are determined in the coordinate-system of the reference-base attached to the calibration phantom using a tracked pointer. The 2D image locations of the fiducials are determined based on the inherent geometric arrangement of the fiducial spheres and image processing steps. Based on simple thresholding and connected-component labeling methods, candidate fiducials are extracted from the image. In order to identify correct fiducial detections and to establish correspondences between all the 2D and 3D fiducial locations, a lookup-table (LUT) based strategy has been developed. A prerequisite for this strategy is the successful detection of one of the line patterns in the top layer of the phantom (Fig. 1). The detected line pattern is then used to normalize all the detected candidate fiducials. These normalized positions are then compared with an off-line generated LUT consisting of simulated fiducial projections with different extrinsic calibration parameters. In order to identify the optimal LUT item, a distance map is computed between all the LUT items and the current set of normalized fiducial positions. Cross-correlation is further applied to identify the precise fiducial positions derived from the optimal LUT-item. The calibration parameters are then computed based on commonly used direct linear transformation method [8]. For detailed information on the phantom detection algorithm we would like to refer to our work [9].

2.2 Patch Statistical Shape Model Construction

Statistical shape models (SSMs) have been originally introduced by Cootes et al. [10] to the field of image processing. Based on a training population of shape instances, its statistical variation can be used to derive new valid shapes. A SSM of the hemi-pelvis (one for each patient side) was constructed from a training population $m = 20$ CT-datasets. Surface model instances were semi-automatically segmented and extracted using Amira software (Visage Imaging, Richmond, Australia). Direct correspondences between the instances were established using diffeomorphic demons algorithm [11]. The intensity-based method was used to register the binary segmentation volumes of the corresponding pelvis surface models, whereas each aligned surface instance $X^{I,r}$ consists of N 3D vertices:

$$X^{I,r} = \{X_0^{I,r}, Y_0^{I,r}, Z_0^{I,r}, \ldots, X_n^{I,r}, Y_n^{I,r}, Z_n^{I,r}, \ldots, X_{N-1}^{I,r}, Y_{N-1}^{I,r}, Z_{N-1}^{I,r}\} \quad (1)$$

where I denotes the specific instance and $r \in \{\text{left, right}\}$ represents the pelvis side. Principal component analysis (PCA) was then applied to the aligned training population to explore the statistical variability (Fig. 2). For a proper clinical diagnosis of FAI related problems, the main interest is in the 3D shape of the hip joint. Hence, the focus here is on the 3D reconstruction of the acetabular shape. In order to accomplish this, an acetabular patch-SSM was constructed for each patient side. The patch-SSM concept has been originally introduced in [12][13] in order to guide the matching of a pelvis-SSM to sparse ultrasound data. In the present study, we will apply it for reconstruction of 3D acetabular surface models from 2D calibrated X-ray images.

Based on the mean hemi-pelvis model $\overline{X}^r$ of the training population, the acetabulum patch was interactively defined. Thereby, mainly the fossa region

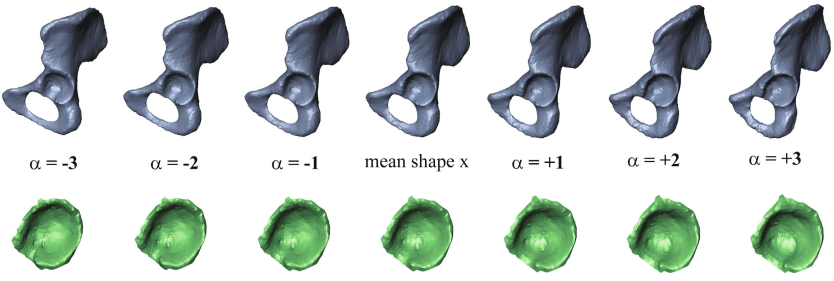

Fig. 2. First eigenmode of variations of the left hemi-pelvis (first row) and of the left acetabulum-patch (second row), generated by evaluating $y + \alpha\sqrt{\lambda_j}p_j$ with $\alpha \in \{-3, \ldots, +3\}$, $y = \{\overline{X}, \overline{q}\}$, eigenvectors p_j and eigenvalues λ_j

and the acetabular rim were selected as shown in Fig. 1, resulting in a list of K numbered vertices:

$$v^r = \{v_0^r, v_1^r, \ldots, v_k^r, \ldots, v_{K-1}^r\} \tag{2}$$

where $v_k = \{n\}$. As correspondences between all training instances were established in a previous step (Eq. 1), an acetabulum surface patch $q^{I,r}$ could be extracted from the associated hemi-pelvis model $X^{I,r}$ using the list of numbered vertices:

$$q^{I,r} = \{q_0^{I,r}, q_1^{I,r}, \ldots, q_k^{I,r}, \ldots, q_{K-1}^{I,r}\} \tag{3}$$

where $q_k^{I,r} = \{X_{v_k^r}^{I,r}, Y_{v_k^r}^{I,r}, Z_{v_k^r}^{I,r}\}$. In order to compensate for the inherent translational differences of the patch instances $q^{I,r}$, another registration step was performed. This step is required for capturing the local shape variations of the acetabulum. Therefore, the mean patch model $\overline{q}^r$ was extracted from the mean hemi-pelvis model $\overline{X}^r$ according to Eq. 3:

$$\overline{q}^r = \{\overline{q}_0^r, \overline{q}_1^r, \ldots, \overline{q}_k^r, \ldots, \overline{q}_{K-1}^r\} \tag{4}$$

where $\overline{q}_k^r = \{\overline{X}_{v_k^r}^r, \overline{Y}_{v_k^r}^r, \overline{Z}_{v_k^r}^r\}$. In the following, each patch instance $q^{I,r}$ was rigidly registered to the mean patch $\overline{q}^r$. Afterwards, PCA was applied again to reveal the statistical variability. The first eigenmode of the acetabulum patch-SSM is depicted in Fig. 2.

2.3 3D Acetabular Shape Reconstruction

In the following description, we denote the bone edges extracted from the 2D X-ray images as contours and the corresponding apparent contours extracted from a 3D model (mean surface model or an instantiated model) as silhouettes.

Feature Extraction. In order to register a SSM to the X-ray radiographs, certain pelvic features have to be extracted from both images. After calibrating both images, the anterior superior iliac spine (ASIS), the pubis symphysis and the posterior inferior iliac spine (PIIS) landmarks of the respective hemi-pelvis

have to be defined on both radiographs. As these landmarks are normally difficult to identify in the axial image, the landmarks are first determined in the AP image. As a calibration is available, we could find the epipolar lines of these landmarks on the axial radiograph [8]. These epipolar lines can be used to guide the identification of the corresponding landmarks in the axial image (top-left image in Fig. 3).

Moreover, certain pelvic contours need to be defined semi-automatically. This step is performed using live-wire algorithm as implemented in VTK-library[1]. The following four image contours of the respective hemi-pelvis need to be determined (top row images of Fig. 3):

- o contour of hemi-pelvis
- o anterior contour of the acetabular rim
- o posterior contour of the acetabular rim
- o contour of acetabular fossa

Hierarchical Patch-SSM Based Registration. After the semi-automatic extraction of the pelvic features, the remaining steps of statistical shape model registration are automatically performed. In the first place, the mean hemi-pelvis model $\overline{X}^r$ is registered to the X-ray scene using paired-point matching. The corresponding landmarks (see previous section 2.3) were predefined based on the mean hemi-pelvis model and used to compute the affine transformation from the hemi-pelvis SSM space to the X-ray space. The alignment of the hemi-pelvis SSM was further improved based on the 3-stage approach by Zheng et al. [14]. This approach is based on finding correspondences between the silhouettes of the surface model (here: the silhouettes of the mean hemi-pelvis model $\overline{X}^r$) and the 2D outer contours of the projected surface model (here: the contours of the hemi-pelvis defined in both X-ray images). These correspondences are then used to estimate the affine transformation between the two spaces. This registration step is followed by a statistical instantiation and regularized non-rigid deformation. After completion of the 3-stage based alignment, an optimal match of the hemi-pelvis SSM to the X-ray scene is achieved. However, the match is only based on the outer contour of the pelvis, as extracted from the X-ray images.

In order to improve the fitting around the acetabular region, information on additional contours of the acetabulum needs to be integrated. Besides the anterior and posterior acetabular rim contours also the fossa contour can be identified. As the fossa of the hemi-pelvis does not provide a visible silhouette, matching cannot be established. Therefore, the instantiated hemi-pelvis model is replaced by the mean surface model of the acetabular patch-SSM based on the direct correspondences according to Eq. 3. This localized patch-SSM is more suitable to be registered to the additional X-ray contours of the acetabulum, as all the relevant silhouettes can be easily extracted.

After aligning the patch-SSM with respect to the X-ray scene based on the instantiated hemi-pelvis model, a scaled rigid transformation based on the

[1] Visualization Toolkit; `www.vtk.org`

anterior and posterior acetabular rim contours and their corresponding silhouettes is further estimated. These silhouettes were defined a priori based on the mean patch model and were used to establish correspondences with the respective contours defined in X-ray images. It was found that an initial scale estimation is critical for an accurate reconstruction of the acetabular surface model. In the present study, this was done as follows. All the anterior and posterior acetabular rim contours (silhouettes) in X-ray (SSM-) space were treated as one point set, whereas the unit of the contour points is in *pixels* and the unit of the silhouette points is in *mm*. For each of the three point sets (there were 2D contour point sets, one from the AP image and the other from the axial image, and one 3D silhouette point set from the mean patch model), the first principal axis was computed. Subsequently, the points were projected on this principal axis and the distances $d_c^{AP,axial}$ ($d_s^{AP,axial}$) between two contour (silhouette) points farthest away along the axis were determined. The average distance d_c for both images was further multiplied by the pixel scaling factor, determined from the calibration procedure, to convert it from *pixel* to *mm* unit. The initial scale was then determined as the ratio between d_c and d_s.

In order to recover the acetabular depth, the registration is further extended by involving the fossa region. Correspondences of the fossa region in X-ray and SSM-space are determined iteratively. For each step, all points of the fossa contour in X-ray space are backprojected using the calibration matrix, resulting in 3D rays. For each ray, the distances to all mean patch model vertices are computed. The vertex with minimal Euclidean distance to the 3D ray is taken as corresponding point to the respective fossa contour point in X-ray space. Together with the corresponding point pairs of the anterior and posterior acetabular rim points, an affine registration is computed to update the position and scale of the mean patch model with respect to all three contours. The 3D reconstruction of the acetabulum is completed by statistical instantiation [15] of the patch-SSM taking all three contours into consideration.

2.4 Experiments and Results

The proposed hierarchical strategy for acetabulum reconstruction was tested on six cadaveric bones (none of the bones was involved in the SSM construction process). Six pairs of X-ray radiographs (anterior-posterior and cross-table axial) were acquired, whereas both hip joints were considered for reconstruction of the acetabulum. Prior to the X-ray acquisition, the calibration phantom, the femur bone and the pelvis were equipped with passive reference bases and tracked during acquisition by an infrared camera system (Polaris, NDI, Canada), as the bones and the phantom were subject to movement during the image acquisition. The acquired images were calibrated individually with respect to the coordinate system established by the reference base attached to the pelvis and the features were semi-automatically determined according to section 2.3. While the determination of the landmarks and acetabular contours took about 1 minute per image, the extraction of hemi-pelvis contours took about 2-3 minutes per image.The 3D reconstruction of the acetabular surface was then performed au-

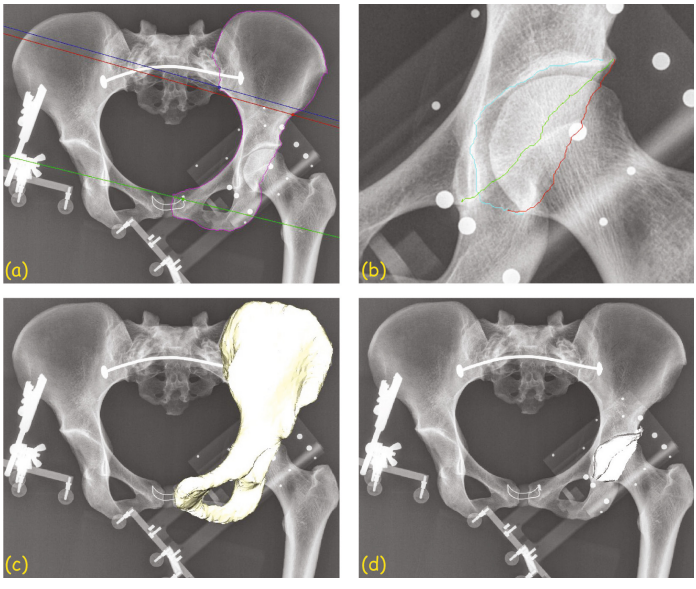

Fig. 3. Hierarchical 2D/3D reconstruction strategy: (a) contour of hemi-pelvis and landmarks with epipolar lines (green: pubis symphysis, red: ASIS, blue: PIIS) (b) acetabular contours (red: posterior rim contour, green: anterior rim contour, cyan: acetabular fossa contour) (c) registered hemi-pelvis SSM (d) registered acetabular patch-SSM

tomatically as described in section 2.3. In order to determine the reconstruction accuracy, CT-scans of the cadaveric pelvises were acquired. The pelvic surface models were extracted from the associated CT-scans and the correspondences between these surface models and the associated mean hemi-pelvis model were established using diffeomorphic demons algorithm [11]. Analogously, acetabulum patches were extracted for both sides and further served as ground truth for validation. On the basis of the direct correspondences, the ground truth acetabulum was rigidly registered to the corresponding reconstructed 3D acetabular surface. The reconstruction accuracy was then assessed using MESH-tool [16], which uses the Hausdorff distance to estimate the distance between triangular 3D meshes. Two experiments were performed to evaluate the efficacy of the present approach.

In the first experiment, the accuracy of deriving the acetabular surface models only based on the hemi-pelvis reconstruction was evaluated. For each case, an acetabulum patch was directly extracted from the reconstructed hemi-pelvis model based on direct correspondences (Eq. 3). In the second experiment, we analyzed the accuracy of the present method. For each experiment, twelve reconstructed acetabular surface models were obtained and compared to the associated ground truth surface models. An overview of the complete error distribution of the twelve reconstructed acetabular surface models in each experiment is presented with box plot. The box plot in Fig. 4 represents the error distribution

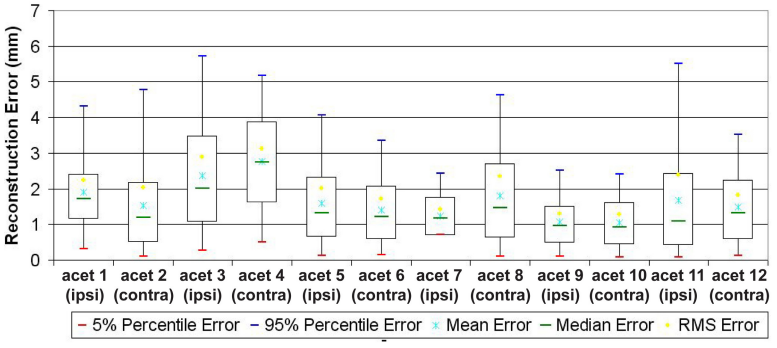

Fig. 4. Box plot indicating the accuracy of the twelve acetabular surface models extracted from the reconstructed hemi-pelvis models

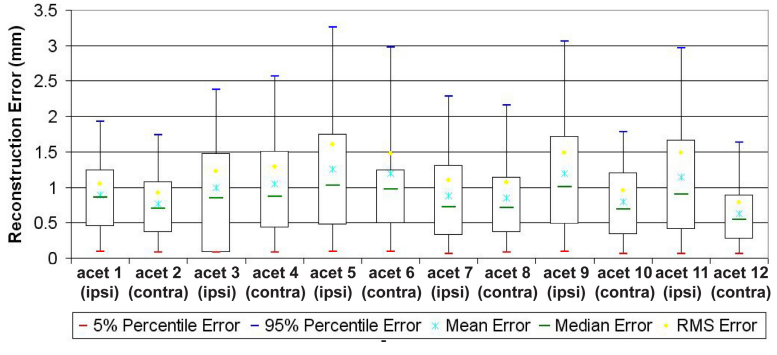

Fig. 5. Box plot indicating the accuracy of the present method

of the first experiment, while Fig. 5 shows the error distribution of the second experiment. For all datasets the mean error, root mean squared (RMS) error as well as the 5%, 25%, 50%, 75% and 95% percentile errors were computed. The average mean error of the 12 acetabular surface models obtained from the reconstructed hemi-pelvis models was 1.659 ± 0.508 mm and this error decreased to 0.970 ± 0.198 mm when the present method was used. On average, the present method improved the reconstruction accuracy by 0.688 mm. It was found that the present method unanimously improved the acetabular surface model reconstruction accuracy for almost all datasets except one dataset (*acet9*), where the accuracy was slightly worse. Regions of error occurred either in the fossa (dataset *acet2* in Fig. 6), or at the cutting edge of the patch (dataset *acet12* in Fig. 6), but rarely along the acetabular rim (dataset *acet1* in Fig. 6).

The X-ray image acquisition was always focused on one pelvis side. The calibration phantom was arranged with respect to the hip joint of the focused side (e.g. left patient side in Fig. 3). In order to investigate an impact of calibration phantom positioning on the reconstruction accuracy, the reconstruction errors

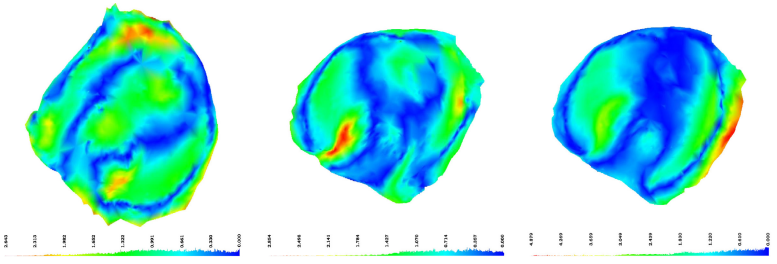

Fig. 6. Analysis of reconstruction accuracy using MESH-tool [16]. The error values are superimposed on the reconstructed acetabular surface models. Datasets, depicted from left to right: acet1, acet2 & acet11.

of ipsi- (when phantom was positioned close to the acetabulum to be reconstructed) and contralateral (when phantom was positioned on contralateral side of the pelvis) side were compared. While the mean reconstruction error for the ipsilateral cases is 1.061 ± 0.159 mm, the mean error for the contralateral cases is 0.879 ± 0.203 mm. For the acquired six datasets, the reconstruction is slightly better for the contralateral side although the exact reason for this needs to be carefully analyzed in the future when more data will be available.

3 Discussion

A 3D reconstruction of the hip joint from conventional X-ray radiographs would have an enormous benefit for the diagnosis and planning of FAI-related issues. Therefore, we proposed a method for X-ray calibration and subsequent acetabular 2D/3D reconstruction. We developed a mobile X-ray calibration phantom, which can be placed anywhere next to the hip joint. It does not interfere the image acquisition and is thus regarded as clinically acceptable. The calibrated images are use to semi-automatically extract relevant pelvic features. The non-rigidly registered hemi-pelvis model is then used to guide the matching of a localized patch-SSM of the acetabulum. Based on the 2D detected acetabular contours, the patch-SSM is optimally fitted to contours extracted from the X-ray images. The proposed method was evaluated based on twelve datasets, acquired from six cadaveric hip joints, showing reasonably good results. Though the clinical significance has not been evaluated, a more accurate reconstruction of the acetabular surface will definitely have a positive impact on the clinical decision.

The main drawbacks of our approach are the user interactivity for contour detection and the required tracking of the patient. However, as a live-wire based semi-automatic method was used to extract the relevant contours, the manual burden on the surgeon is low. Also the presence of soft tissue in clinical cases and possible occlusions of anatomical features by the calibration phantom should not affect the contour extraction, assuming a careful user interaction. The tracking requirement can be omitted by maintaining a fixed relationship between the calibration phantom and the patient.

References

1. Wicky, S., Blaser, P., et al.: Comparison between standard radiography and spiral CT with 3D reconstruction in the evaluation, classification and management of tibial plateau fractures. Eur. Radiol. 10, 1227–1232 (2000)
2. Mitton, D., Zhao, K.: 3D reconstruction of the ribs from lateral and frontal x-rays in comparison to 3D CT-scan reconstruction. J. Biomech. 41, 706–710 (2008)
3. Tannast, M., Siebenrock, K., Anderson, S.: Femoroacetabular impingement: Radiographic diagnosis - what the radiologists should know. AIH Am. J. Roentgenol. 188, 1540–1552 (2007)
4. Krekel, P., Vochteloo, A., et al.: Femoroacetabular impingement and its implications on range of motion: a case report. J. Med. Case Reports 5 (2011)
5. Tannast, M., Goricki, D., et al.: Hip damage occurs at the zone of femoroacetabular impingement. Clin. Orthop. Relat. Res. 466, 273–280 (2008)
6. Beaule, P., Zaragoza, E., et al.: Three-dimensional computed tomography of the hip in the assessment of femoroacetabular impingement. J. Orthop. Res. 23, 1286–1292 (2005)
7. Zheng, G., Schumann, S.: 3D reconstruction of a patient-specific surface model of the proximal femur from calibrated x-ray radiographs: a validation study. Med. Phys. 36, 1155–1166 (2009)
8. Hartley, R., Zisserman, A.: Multiple view geometry in computer vision, 2nd edn. Cambridge University Press (2004)
9. Schumann, S., Dong, X., et al.: Calibration of C-arm for orthopedic interventions via statistical model-based distortion correction and robust phantom detection. In: ISBI. IEEE (2012)
10. Cootes, T., Taylor, C., et al.: Active shape models - their training and application. Comput. Vis. Image Underst. 61, 38–59 (1995)
11. Vercauteren, T., Pennec, X., Perchant, A., Ayache, N.: Non-parametric Diffeomorphic Image Registration with the Demons Algorithm. In: Ayache, N., Ourselin, S., Maeder, A. (eds.) MICCAI 2007, Part II. LNCS, vol. 4792, pp. 319–326. Springer, Heidelberg (2007)
12. Schumann, S., Puls, M., Ecker, T., Schwaegli, T., Stifter, J., Siebenrock, K.-A., Zheng, G.: Determination of Pelvic Orientation from Ultrasound Images Using Patch-SSMs and a Hierarchical Speed of Sound Compensation Strategy. In: Navab, N., Jannin, P. (eds.) IPCAI 2010. LNCS, vol. 6135, pp. 157–167. Springer, Heidelberg (2010)
13. Schumann, S., Nolte, L., Zheng, G.: Compensation of sound speed deviations in 3D B-mode ultrasound for intraoperative determination of the anterior pelvic plane. IEEE Trans. on Inf. Technol. in Biomed. 16, 88–97 (2012)
14. Zheng, G., Rajamani, K.T., Nolte, L.-P.: Use of a Dense Surface Point Distribution Model in a Three-Stage Anatomical Shape Reconstruction from Sparse Information for Computer Assisted Orthopaedic Surgery: A Preliminary Study. In: Narayanan, P.J., Nayar, S.K., Shum, H.-Y. (eds.) ACCV 2006. LNCS, vol. 3852, pp. 52–60. Springer, Heidelberg (2006)
15. Rajamani, K., Styner, M., et al.: Statistical deformable bone models for robust 3D surface extrapolation from sparse data. Med. Image Anal. 11, 99–109 (2007)
16. Aspert, N., Santa-Cruz, D., Ebrahimi, T.: MESH: Measuring errors between surfaces using the Hausdorff distance. In: IEEE International Conference on Multimedia and Expo., vol. 1, pp. 705–708 (2002)